Temperature Control for Automated High Frequency Core Loss Testing

Nick J. Kirkby and Mike K. Ranjram
Miniaturized and Advanced Power Electronics Laboratory
Arizona State University
Email: {njk, mranjram}@asu.edu

2024 IEEE Workshop on Control and Modeling for Power Electronics (COMPEL) | 979-8-3503-0723-8/24/$31.00 ©2024 IEEE | DOI: 10.1109/COMPEL57542.2024.10614063

***Abstract*—This paper describes challenges to automated bulk collection of temperature-controlled magnetic core loss data in the 1-20 MHz regime. Oil immersion is shown to alter the small-signal impedance of ML91S and FR67 ferrite cores by more than 5% over part of their rated frequency ranges which prevents accurate estimation of core loss. Air-based thermal forcing is shown to be a viable alternative to oil for core temperature regulation in high frequency core loss testers. Temperature regulation to $25 \pm 3°C$ is demonstrated on FR80 at 1 MHz up to 1.25 W of dissipation.**

I. Introduction

Optimizing a high-frequency magnetic component for low losses is difficult. Magnetic core loss is known to vary with flux conditions, temperature, core material and geometry. Loss data in manufacturer-provided data sheets are too sparse to locate optimal conditions. Additionally, details on part-to-part or batch-to-batch variation of loss are nonexistent. Finally, quantitative theoretical models are not suitable for practical engineering use. Any such models require accurate knowledge of the specific core material produced by the specific manufacturer to be accurate. This is in contrast to conduction loss, where bulk material properties are well understood, well catalogued, and straightforward to incorporate into estimates. A viable path for mitigating these issues and minimizing core loss in a high-frequency magnetic component is to experimentally estimate it for every flux condition and temperature of interest.

A. Role of Core Loss Models in Power Converter Design Optimization

Figure 1 shows the role of power magnetic loss models in power converter design optimization. When designing a power converter it is desirable to explore the effects of specific design choices on high-level metrics such as efficiency, weight and volume. Accurate core loss models provide a clearer picture of the true value of high frequency operation. This accuracy is needed especially when devising new approaches for miniaturized high-frequency magnetics such as [1]. For example, [2] demonstrates that FR67 achieves high performance factor in the 10 MHz regime. However, pushing converters to such high frequencies is challenging, requiring new design insights and careful understanding of bleeding-edge power semiconductor device technologies [3], [4]. These difficulties of higher frequency operation are taken on because of the miniaturization opportunity that they bring to volume-dominant magnetic components in power converters. Assessing these difficulties and opportunities during the design and conceptualization phases requires accurate core loss data that is, ideally, fully parameterized over the operating range of interest.

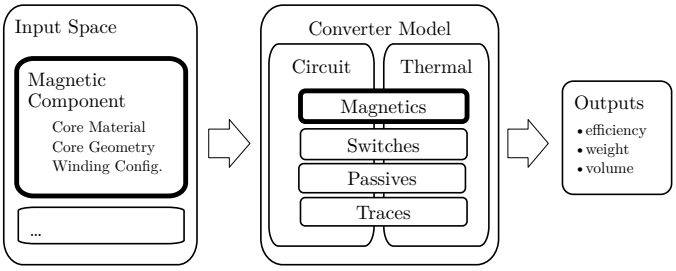

Fig. 1: Role of magnetics models in converter optimization.

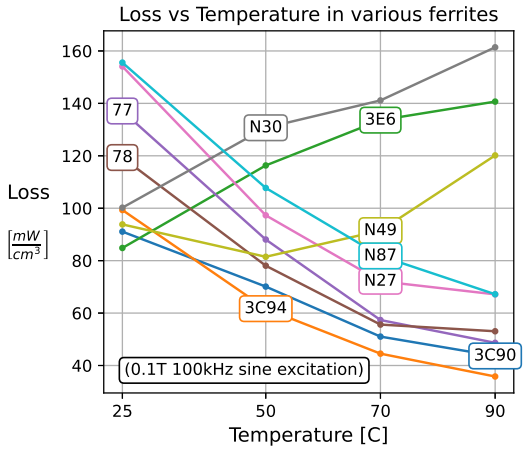

Fig. 2: Loss vs. Temperature in various ferrites at 100kHz. Data from MagNet [5]–[7].

B. Necessity of Temperature Control in Core Loss Testers

Core losses in ferrites vary substantially with temperature. Figure 2 shows that volumetric core loss varies by +/-60% over the temperature range 25°C to 90°C for some types of ferrite.

Because core loss may vary substantially with temperature it is essential that core temperature is both measured and controlled during data acquisition. The automated resonant

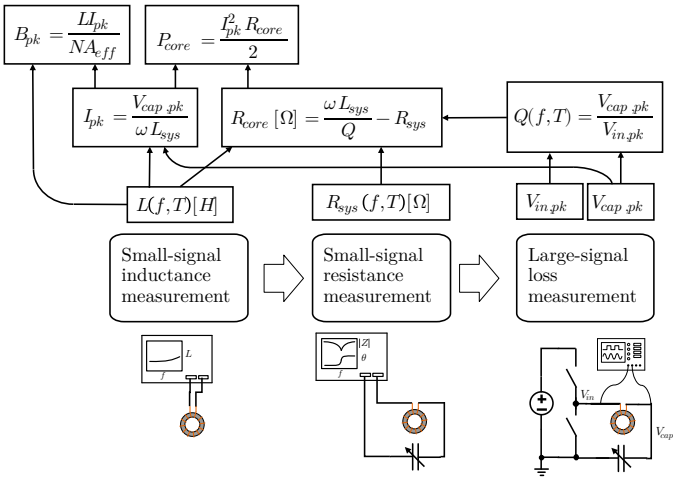

Fig. 3: One possible implementation of the resonant core loss estimation method described in [9].

method of core loss testing described in [8], [9] requires three sets of electrical measurements to be made. These measurements and one possible interpretation of their relation to core loss and peak flux is shown in Figure 3. Note that P_{core} depends on all three sets of electrical measurements in addition to intermediary modeling assumptions. It is therefore imperative that core temperature is regulated and reported in each measurement step [1].

C. Necessity of Core Loss Test Automation

Core loss varies as a function of multiple factors. Core loss data must therefore be independently parameterized by each factor such that their effects may be observed independently. Consider sweeping three factors: flux amplitude, frequency, and temperature at a granularity of ten points per factor. This will result in a dataset of size 10^3 observations. Generally for a search space of K factors each uniformly distributed over N intervals the total number of observations goes as $O = K^N$. Core loss data is most useful in the early design phase, therefore it is desirable to have comparative data for various core materials and also geometries. Depending on the application, additional flux parameters such as dc bias and wave shape may also be of interest, further increasing the number of required observations. The consistency and speed required to make upwards of 10^3 observations in a reasonable engineering timeline creates the need for automation.

The current state-of-the-art in automated core loss data collection is [5]–[7] which achieves 3000 points per hour of temperature-controlled operation. However due to its use of oil as a cooling medium this method is not directly applicable to higher frequency core loss testing (see Section II). Table I compares key metrics of some published core loss test apparatus.

[1]Core loss is referred to as an "estimated" or an "observed" quantity rather than a measured one here to emphasize that it is the combination of multiple electrical measurements and modeling assumptions. In all known core loss estimation methods including volt-amperic, resonant, and calorimetric a set of proxy measurements (voltages and currents or temperatures) are extended by models to arrive at an estimate of core loss.

II. Effects of Oil Immersion on Core Impedance Measurements

Due to its low thermal resistance, oil provides excellent core temperature regulation compared to air. However it may interfere with resonant core loss measurement methods [2], [8], [12] in the 1-20 MHz range. Small signal impedance data for three different magnetic cores alternately immersed in air and oil is shown in Figure 4. The FR67 and ML91S cores were most affected by oil immersion and both exceeded 5% impedance difference relative to air over a large portion of the manufacturer rated operating frequency range.

The measurement procedure is as follows: impedance data were gathered using an Agilent 4294A Impedance Analyzer with its standard 16047E test fixture. Impedance was first measured with the core in air. Next, the core was immersed in approximately 500mL of canola oil in a glass jar. Care was taken to keep the core and its windings in the same relative position as the in-air measurement, and the jar was positioned such that the core was far from the jar walls. Air measurements were then repeated after thoroughly cleaning each core with isopropyl alcohol to remove oil residue. Impedance measurements post-cleaning were found to be consistent with the initial in-air measurements. However, if the oil residue was not thoroughly cleaned some impedance change remained observable on the FR67 and ML91S cores.

Because resonant core loss estimation methods incorporate a small signal impedance measurement, the impedance difference due to oil immersion will result in modeling error if not accounted for. Therefore, either the electrical effects of oil immersion must be modeled or alternate cooling methods must be considered. Owing to its complexity as well as the suitability of the latter approach, modeling the electrical effects of oil immersion is not given further consideration here.

III. Thermal Models for Electrical Core Loss Testers

Thermal circuit models [13] are used to analyze potential solutions to the problem of regulating core temperature during core loss testing. The analysis done in this section answers the question: is forced air a viable temperature regulation solution for high frequency magnetic core loss testers?

A. Generic Thermal Circuit Model

Equation 1 is the steady-state 1D heat equation. It is the thermal circuit analogue to Ohm's Law. It relates a temperature difference $\Delta T[^\circ C]$ to a heat flux $\dot{Q}[W]$ and a thermal resistance $R_{th}[\frac{K}{W}]$

$$\Delta T = \dot{Q} R_{th} \tag{1}$$

Figure 5 shows a thermal circuit model of a magnetic core. In electrical (non-calorimetric) core loss testers T_{core} is regulated in order to make temperature an independent variable in the collected data. The environment (empty) is the subject

Dataset	Size [points]	Rate [points/hr]	Freq. Range [Hz]	Temperature Reported	Temperature Controlled	Fluid	Method
[5]–[7] (2023)	575,009	3000	50k-500k	✓	✓	Oil	Electrical, Volt-amperic
[2] (2016)	738[a]	?	20k-60M	✗	✗	Air	Electrical, Resonant
[8] (2023)	806	?	5M-16M	✓	✗	Air	Electrical, Resonant
[10] (2021)	44	?	5M-50M	✓	✓	Air	Calorimetric, Differential
[11] (2023)	-	45[b]	100k	✓	✓	Novec 7500	Calorimetric, Adiabatic

TABLE I: Temperature reporting in public magnetic core loss datasets.
[a] Data in [2] is provided as Steinmetz parameters. The estimate of 738 points assumes 6 core loss points per Steinmetz parameter set.
[b] The estimate of 45 points per hour is based upon 80 seconds per heat described in [11]. Practically this is a lower bound as cooling time is not included.

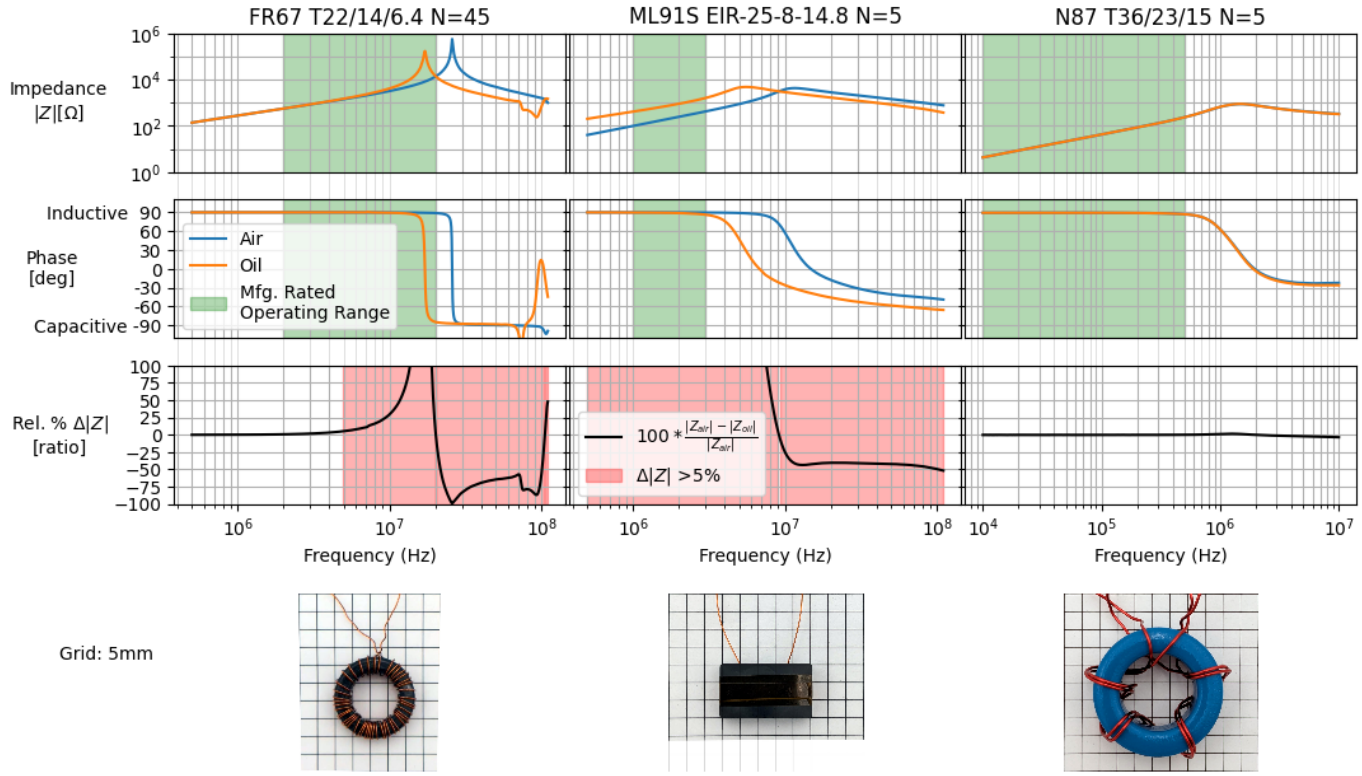

Fig. 4: Impedance vs. frequency for three ferrite cores alternately immersed in air and oil. The manufacturer-recommended operating frequency range of the cores is shaded in green. Frequencies where the impedance of the oil-immersed core differs from the air measurement by more than 5% are shaded in red.

of this design. The values of $R_{th,core}$ and $C_{th,core}$[2] depend on both core material and geometry. Here we consider the nominal case of a T22/14/6.4 ferrite toroid core.

B. Estimating Core Thermal Resistance

Thermal resistance $R_{th}[\frac{K}{W}]$ is an extensive or lumped quantity. It captures material properties as well as geometry. Its corresponding intensive[3] quantity is thermal conductivity

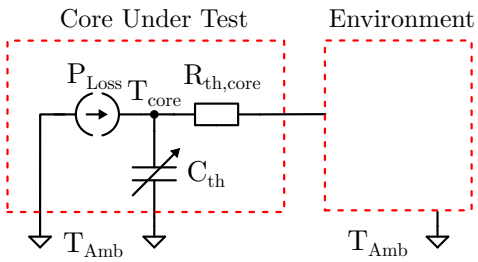

Fig. 5: Generic thermal circuit model for core loss testers. $P_{loss}[W]$ is a heat flux due to core loss, $T_{core}[°C]$ is the temperature of the core, $C_{th}[\frac{J}{K}]$ is the lumped heat capacity of the core and $R_{th}[\frac{K}{W}]$ is the lumped thermal resistance from the core to its surface.

[2] $C_{th,core}$ is drawn as a variable capacitor because the specific heat capacity of ferrite exhibits temperature dependence as described in [10]. Our analysis is concerned with steady-state thermal regulation and so $C_{th,core}$ is left out of subsequent analyses.

[3] Thermal resistance $R_{th}[\frac{K}{W}]$ and electrical resistance $R[\Omega]$ are both extensive or lumped quantities. In contrast, thermal conductivity $k[\frac{W}{m \cdot K}]$ and electrical conductivity $\sigma[\frac{S}{m}]$ are intensive or material properties.

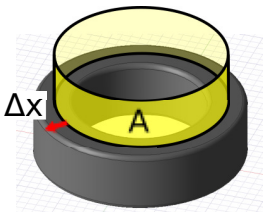

Fig. 6: Approximation of toroid in 1D.

$\Delta x\,[m]$	$A\,[m^2]$	$k_{ferrite}\left[\frac{W}{m*K}\right]$	$\frac{1}{4}R_{th}\left[\frac{K}{W}\right]$
4e-3	0.362e-3	3	0.92

TABLE II: Parameters used to estimate R_{th} of a T22/14/6.4 ferrite toroid using (2). An additional factor of $\frac{1}{4}$ is applied to account for heat flow out of each surface.

$k[\frac{W}{m\cdot K}]$ which is a material property. For ferrite k may be assumed to be isotropic with a value between 1 and 5 $\frac{W}{m\cdot K}$ [14], [15].

$R_{th,core}$ can be estimated by Fourier's Law of Heat Conduction which relates heat and temperature gradients in solids. The core is approximated as a single-dimensional body in Figure 6. Next the 1D form of Fourier's Law

$$R_{th} = \frac{\Delta x}{kA} \tag{2}$$

is used to obtain the thermal resistance of the core $R_{th,core}$. Δx is distance in the direction of heat flow, A is cross-sectional area of the thermal conductor and k is thermal conductivity of the core material. Quantities are shown in Table II. The estimated core thermal resistance is $R_{th,core} \approx 0.92\frac{K}{W}$.

C. Analysis of Core in Ambient Air

This section models the equivalent thermal resistance of air over a toroid $R_{fluid,air}$. A thermal circuit model of a core in ambient air is shown in Figure 7. $C_{th,core}$ has been removed as it does not affect steady-state behavior.

Equation 3 expresses fluid thermal resistance $R_{th,fluid}[\frac{K}{W}]$ in terms of the convective heat transfer coefficient $h[\frac{W}{m^2\cdot K}]$ and surface area $A[m^2]$,

$$R_{th,fluid} = \frac{1}{hA} \tag{3}$$

The convective heat transfer coefficient h is estimated using a Nusselt number correlation. The Nusselt number Nu_{L} is a dimensionless quantity defined as the ratio of convective to conductive heat transfer at a fluid boundary. It is parameterized in terms of a geometry-dependent characteristic length L (the "$_L$" in Nu_{L}) as well as flow velocity and fluid properties such as density, viscosity, thermal conductivity, and specific heat,

$$Nu_{\text{L}} = \frac{h}{k/L} \tag{4}$$

The Nusselt number Nu_{L} is calculated for air at velocities ranging from 0.01 to 1 m/s using the square toroid correlation given in [16, Table 5]. The Nusselt numbers for oil and water

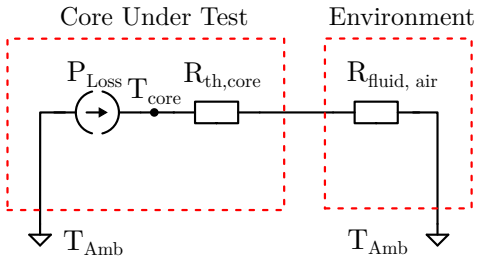

Fig. 7: Thermal circuit model for a core in ambient air.

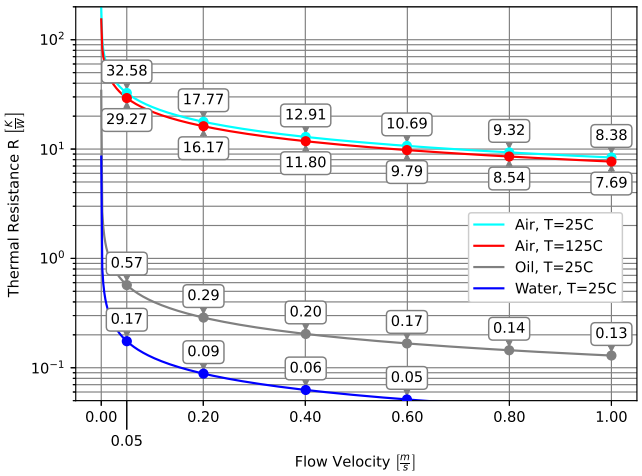

Fig. 8: Thermal resistance from core surface to ambient for air, oil and water in axial flow over a T22/14/6.4 toroid as a function of flow velocity.

are also calculated for comparative purposes. Next, (4) is used to solve for the convective heat transfer coefficient h. Finally (3) is used to express h as an equivalent thermal resistance R_{fluid}.

The resulting thermal resistances are plotted in Figure 8 as a function of flow velocity. The thermal resistance of air is large, approximately 60 times that of oil. The thermal resistance of air has a weak temperature dependence which is assumed to be negligible in subsequent analysis.

For all flow velocities it holds that $R_{fluid,air} \gg R_{th,core}$ where $R_{th,core}$ was estimated to be $0.92\frac{K}{W}$ in Section III-B. Because the thermal resistance of the air is much greater than that of the core it can be assumed that the core will have a negligible internal thermal gradient.

Applying (1) with $\Delta T = T_{core} - T_{amb}$, $\dot{Q} = P_{Loss}$ and $R_{th} = R_{th,core} + R_{fluid,air}$ we obtain,

$$T_{core} - T_{amb} = P_{Loss} \times (R_{fluid,air} + R_{th,core}) \tag{5}$$

Because $R_{fluid,air} \gg R_{th,core}$ it may be assumed that $R_{th} \approx R_{fluid,air}$,

$$T_{core} - T_{amb} = P_{Loss} \times R_{fluid,air} \tag{6}$$

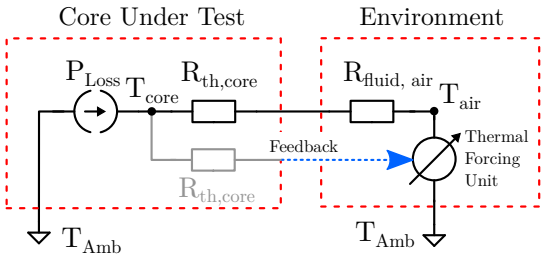

Fig. 9: Thermal circuit model of a core in temperature-controlled air.

High frequency core loss testing in air under continuous electrical excitation is known to result in substantial core temperature rise above ambient. [8] used a fan to maintain a temperature rise under 25°C above ambient. This is consistent with $R_{fluid,air} \approx 12.5\frac{K}{W}$ in Figure 8. (6) shows that in thermal steady state with a fixed ambient temperature and air flow, the core temperature T_{core} is proportional to core loss P_{Loss}. This is problematic because P_{Loss} varies during testing, resulting in a varying T_{core}. This in turn complicates the core loss estimation procedure in Figure 3 because small and large signal measurements are no longer at the same temperature. It is desirable to both measure and regulate T_{core} under changing P_{Loss}, therefore, tighter control of core temperature is required during large-signal core loss testing.

D. Thermal Forcing

The high thermal conductivity and low electrical conductivity of oil make it a desirable passive thermal regulation fluid for core loss testing. However, its use in high-frequency core loss testing is questionable due to the impedance-altering effects described in Section II.

Another approach to air-based core temperature regulation is to modulate the temperature of the air passing over the core. This technique is called thermal forcing or temperature forcing and it is used widely in industry for thermal shock testing of semiconductors and electronic assemblies. The thermal forcing unit blows temperature-controlled air over the core. The core temperature T_{core} is used as a feedback signal to the thermal forcing unit which then adjusts the temperature of its air to force the core to a defined temperature. Figure 9 shows a thermal circuit model of this arrangement. The feedback signal comes from a temperature sensor placed in contact with the core but out of the airflow of the thermal forcing unit.

Thermal forcing regulates core temperature by providing the necessary ΔT to overcome the high thermal resistance of air. This can be modeled by adjusting (6) such that the previously uncontrolled T_{amb} is now a variable T_{air},

$$T_{core} - T_{air} = P_{Loss} \times R_{fluid,air} \tag{7}$$

From (7) a lower limit on controllable core temperature under maximum loss may be found. For example, substituting $P_{Loss,max} = 2W$, $R_{fluid,air} = 12.5\frac{K}{W}$ and $T_{air,min} = -20°C$ we estimate a $T_{core,min} \approx 5°C$.

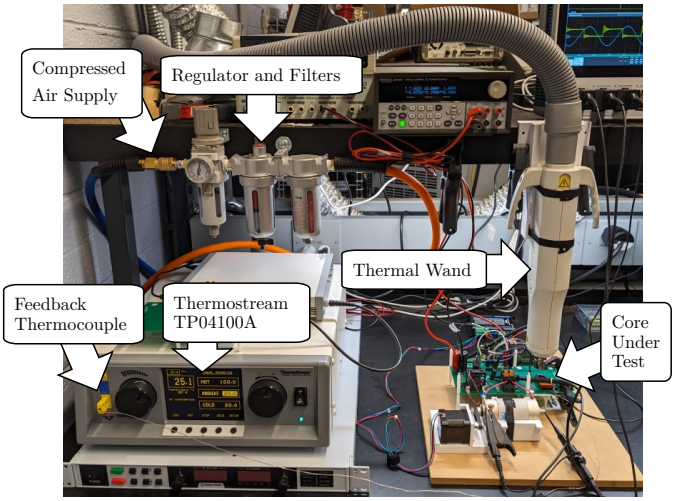

Fig. 10: Overview of experimental setup.

IV. Experimental Validation of Thermal Forcing

The analysis presented in Section III indicates that thermal forcing can be a viable approach for core temperature regulation in high frequency automated core loss testing.

A. Experimental Setup

A Thermostream TP04100A (1998) thermal forcing unit is procured. It is capable of closed-loop thermal control and the achievable air temperature is found to range from -20°C to 220°C. It requires a 90 PSI compressed air supply and standard 1ϕ ac power. Additional items including air filters, a pressure regulator, hoses and fittings are also required. Despite its age, the TP04100A contains a SCPI-compliant serial interface and is amenable to remote control. The unit as installed is shown in Figure 10. Temperature-controlled air exits downwards from the tip of the thermal wand and flows over the core under test.

Figure 11 shows details of the core mounting. A thermocouple is used to measure the temperature of the core under test. This core temperature is used as feedback by the thermal forcing unit. It is important for stable regulation that the thermocouple has low-resistance thermal contact with the core and is not exposed to airflow. The thermocouple is passed through a small hole in a piece of silicone foam placed beneath one side of the core. The approximate path of the thermocouple is shown as a yellow dotted line. The purpose of the foam is to prevent airflow around the thermocouple while being electrically similar to air. Finally, a strip of FR4 fiberglass sheet attached to a clamp is used to hold the core securely in place. Because the silicone foam is a good thermal insulator it is desirable to minimize its contact area with the core, exposing as much as possible of the core surface to airflow.

The same core mounting technique is used for all three types of electrical measurement: small-signal inductance, small-signal resistance, and large-signal loss shown in Figure 3. Because core properties such as permeability may be highly temperature dependent, the thermal forcing unit is used to

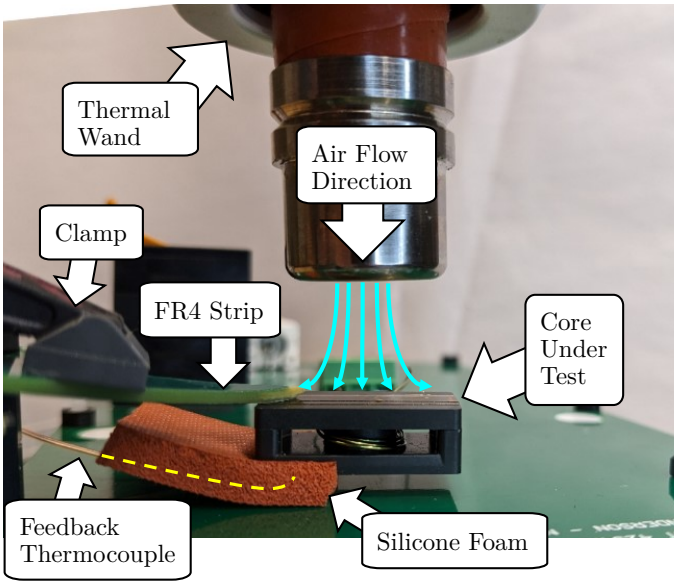

Fig. 11: Detail of core mounting and thermocouple routing.

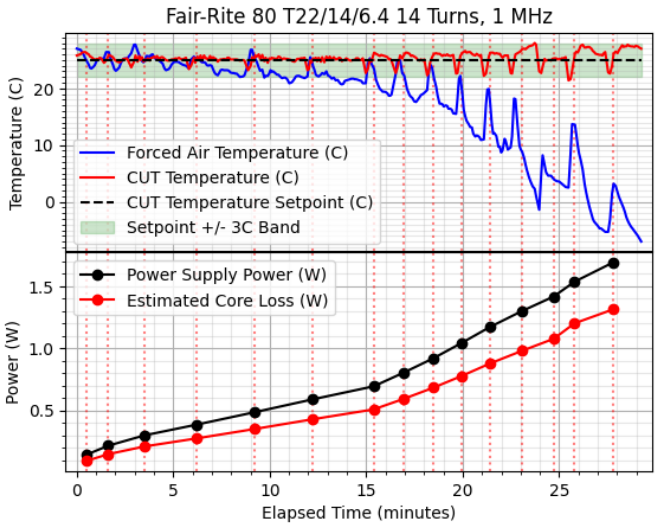

Fig. 12: Forced-air temperature control on FR80 at 1 MHz.

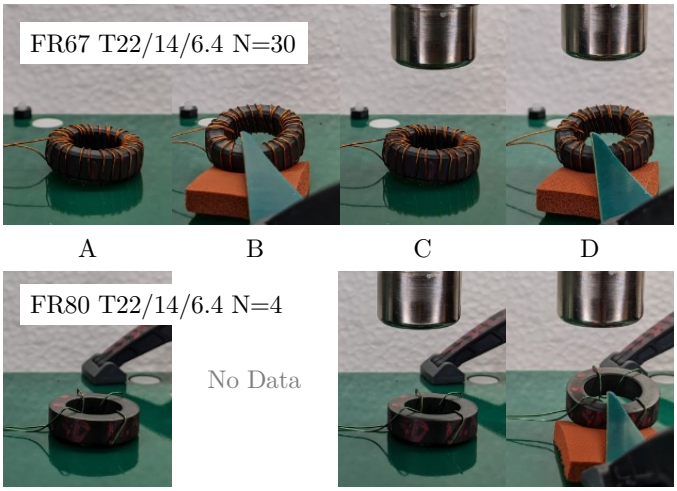

Fig. 13: Various core mounting configurations used for comparative small-signal impedance measurements. The labels "A,B,C,D" correspond to the data shown in Figure 14.

bring the core to a consistent temperature setpoint for all three electrical measurements.

B. Experimental Results

Figure 12 shows temperature and core loss data collected on FR80 material at 1 MHz. The core under test (CUT) temperature as measured by the thermocouple mounted beneath the core is shown to be stable within $\pm 3°C$ over the duration of the test. At higher core loss levels the forced air temperature drops below $0°C$ to maintain a steady core temperature near $25°C$ during $P_{loss} > 1W$ conditions. The core is continuously electrically excited for the duration of the test. The fluctuation in core temperature and corresponding fluctuation in forced air temperature is due to the test technique. Each recorded loss point in the lower plot actually consists of many electrical measurements made near the resonant operating point as the tester finds resonance. Power into the dc bus feeding the tester as measured by the power supply is also plotted as "Power Supply Power (W)". This serves as an upper bound on the core loss estimate. Because all of this power is converted to heat in different parts of the tester, it shows comparatively what fraction of the power is estimated to be attributable to core loss.

Using Figure 12, the effective thermal resistance from core to air may be estimated by dividing the difference between core temperature and forced air temperature by the estimated core loss. By $R_{th} = \frac{\Delta T}{\dot{Q}}$, we find an experimental $R_{th} \approx 25\frac{K}{W}$ at $P_{Loss} = 1W$. This on the higher end of the range of thermal resistances predicted in Figure 8. It is possible that better enclosure design and core mounting could further reduce this thermal resistance.

The current automation achieves one large-signal core loss observation at a period of approximately 112 seconds or 32 points per hour. Test equipment communication is the present speed bottleneck and this is expected to improve substantially with further software optimization.

An additional thermal performance gain can be had by not continuously exciting the core. The time to reach electrical steady state is much shorter than the thermal dynamics. In this way the average power may be greatly reduced without compromising electrical measurements.

C. Electrical Effects of Core Mounting

In Section II it was shown that oil immersion significantly affects the apparent electrical characteristics of the core under test. Similar comparative small-signal impedance measurements were made on the air-based solution check sensitivity to variations in mounting. Ideally the fashion in which the core is fixed to the tester should not affect electrical measurements. Four mounting configurations were tested as

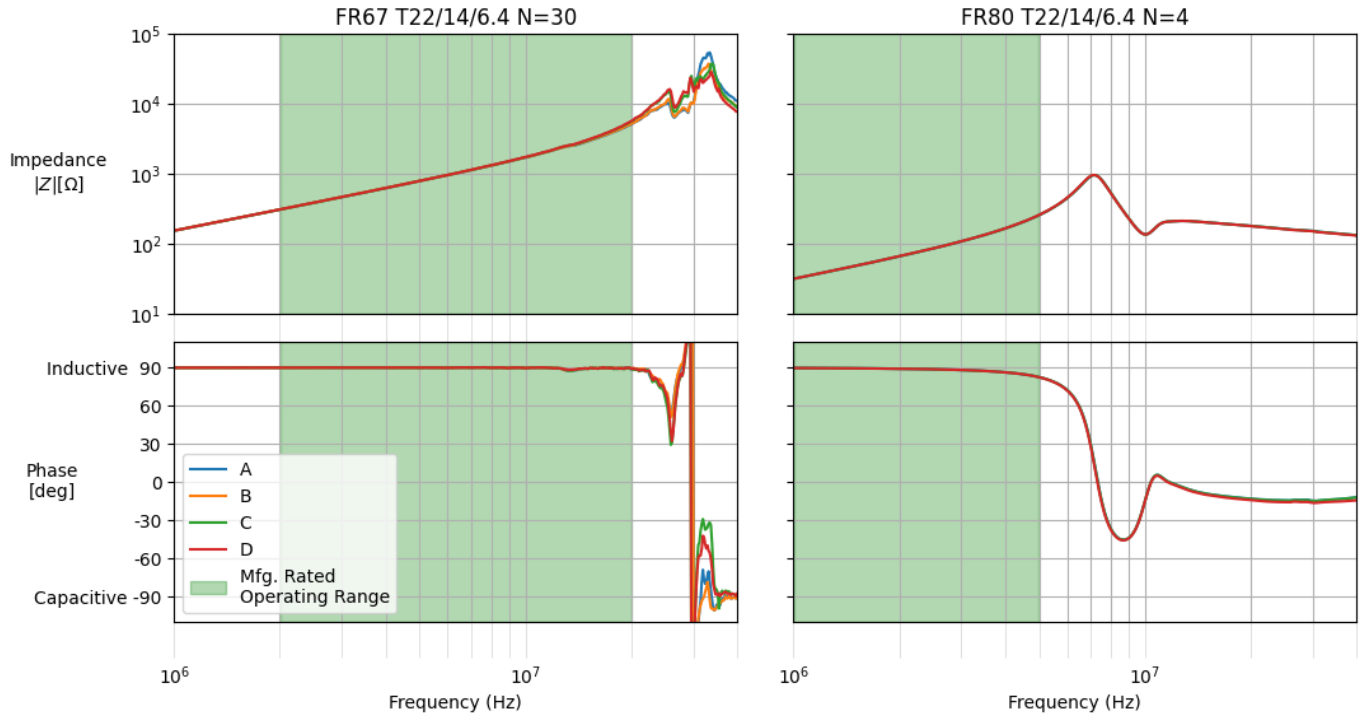

Fig. 14: Impedance vs. frequency for two cores in four different core mounting configurations labelled "A,B,C,D" corresponding to those shown in Figure 13.

shown in Figure 13 and corresponding comparative small-signal impedance data is shown in Figure 14. The items in close proximity to the core including the silicone foam, the FR4 strip, the thermocouple, and the thermal forcing unit nozzle have been found to have negligible impact on the small signal measurements. Namely, the self-resonant frequency of the core (approximately 30 MHz for the FR67 sample and 7 MHz for the FR80 sample shown in Figure 14) remains the same regardless of the mounting configuration. This is in contrast to oil immersion which was observed to reduce the self-resonant frequency significantly on FR67 and ML91S cores.

Data in 14 is gathered with a Bode 100 impedance analyzer in one-port mode connected via 0.5 meters of RG58 coaxial cable to the PCB shown in Figure 11. Short-circuit, open-circuit, and load calibration are done at the core connection terminals. Impedance magnitude and phase measurements of a 47 Ω resistor installed at the core connection terminals are found to be repeatable to within $47\Omega \pm 1\%$ and $0° \pm 0.5°$ over the range 100 kHz to 40 MHz.

V. Conclusion

This paper presents the use of forced air to achieve core temperature regulation in high frequency magnetic core loss testers. The development of novel miniaturized advanced power electronics is shown to require more and higher quality temperature-controlled core loss data, and the challenges of temperature control and test automation are discussed. Small signal impedance measurements on FR67 and ML91S cores immersed in oil show that the use of oil for temperature regulation in high frequency core loss testers is questionable because it alters the apparent electrical characteristics of the core under test. Next, the problem of core temperature regulation is modeled with thermal circuits to arrive at key insights about the thermal resistances R_{th} of ferrite and cooling fluids. Air-based thermal forcing using a Thermostream TP04100A is experimentally validated to effectively regulate core temperature on a FR80 T22/14/6.4 (N=14) toroid at 1 MHz with 1.25 W of estimated core loss. Finally, comparative impedance measurements of show that the air-based approach does not impact the apparent impedance characteristics of FR67 and FR80 magnetic cores and is insensitive to mounting configuration. The use of air-based thermal forcing is deemed suitable for temperature regulation in high-frequency magnetic core loss testers.

References

[1] M. K. Ranjram, I. Moon, and D. J. Perreault, "Variable-Inverter-Rectifier-Transformer: A Hybrid Electronic and Magnetic Structure Enabling Adjustable High Step-Down Conversion Ratios," *IEEE Transactions on Power Electronics*, vol. 33, no. 8, pp. 6509–6525, Aug. 2018. [Online]. Available: https://ieeexplore.ieee.org/document/8264814/

[2] A. J. Hanson, J. A. Belk, S. Lim, C. R. Sullivan, and D. J. Perreault, "Measurements and Performance Factor Comparisons of Magnetic Materials at High Frequency," *IEEE Transactions on Power Electronics*, vol. 31, no. 11, pp. 7909–7925, Nov. 2016. [Online]. Available: http://ieeexplore.ieee.org/document/7370781/

[3] B. J. Galapon, A. J. Hanson, and D. J. Perreault, "Measuring Dynamic On Resistance in GaN Transistors at MHz Frequencies," in *2018 IEEE 19th Workshop on Control and Modeling for Power Electronics (COMPEL)*. Padua: IEEE, Jun. 2018, pp. 1–8. [Online]. Available: https://ieeexplore.ieee.org/document/8460051/

[4] J. Zhuang, G. Zulauf, J. Roig-Guitart, J. Plummer, and J. Rivas, "Small- and Large-Signal Dynamic Output Capacitance and Energy Loss in GaN-on-Si Power HEMTs," *IEEE Transactions on Electron Devices*, vol. 68, no. 4, pp. 1819–1826, Apr. 2021. [Online]. Available: https://ieeexplore.ieee.org/document/9380488/

[5] H. Li, D. Serrano, S. Wang, and M. Chen, "MagNet-AI: Neural Network as Datasheet for Magnetics Modeling and Material Recommendation," *IEEE Transactions on Power Electronics*, vol. 38, no. 12, pp. 15 854–15 869, Dec. 2023. [Online]. Available: https://ieeexplore.ieee.org/document/10232911/

[6] D. Serrano, H. Li, S. Wang, T. Guillod, M. Luo, V. Bansal, N. K. Jha, Y. Chen, C. R. Sullivan, and M. Chen, "Why MagNet: Quantifying the Complexity of Modeling Power Magnetic Material Characteristics," *IEEE Transactions on Power Electronics*, vol. 38, no. 11, pp. 14 292–14 316, Nov. 2023. [Online]. Available: https://ieeexplore.ieee.org/document/10169101/

[7] H. Li, D. Serrano, T. Guillod, S. Wang, E. Dogariu, A. Nadler, M. Luo, V. Bansal, N. K. Jha, Y. Chen, C. R. Sullivan, and M. Chen, "How MagNet: Machine Learning Framework for Modeling Power Magnetic Material Characteristics," *IEEE Transactions on Power Electronics*, vol. 38, no. 12, pp. 15 829–15 853, Dec. 2023. [Online]. Available: https://ieeexplore.ieee.org/document/10232863/

[8] J. R. Anderson and M. K. Ranjram, "Automation of High-Frequency Magnetic Core Loss Data Collection," in *2023 IEEE 24th Workshop on Control and Modeling for Power Electronics (COMPEL)*. Ann Arbor, MI, USA: IEEE, Jun. 2023, pp. 1–8. [Online]. Available: https://ieeexplore.ieee.org/document/10221076/

[9] J. R. Anderson, N. J. Kirkby, and M. K. Ranjram, "Class-D Amplifier-Based Core Loss Measurements for High Frequency Magnetic Materials," pp. 1–8, Jun. 2024.

[10] P. Papamanolis, T. Guillod, F. Krismer, and J. W. Kolar, "Transient Calorimetric Measurement of Ferrite Core Losses up to 50 MHz," *IEEE Transactions on Power Electronics*, vol. 36, no. 3, pp. 2548–2563, Mar. 2021. [Online]. Available: https://ieeexplore.ieee.org/document/9169835/

[11] J. Reynvaan, M. Pajnić, and J. Krenn, "Evaluating Fluid Based Transient Calorimetric Method for Measurement of the Ferrite Core Losses," in *2023 11th International Conference on Power Electronics and ECCE Asia (ICPE 2023 - ECCE Asia)*. Jeju Island, Korea, Republic of: IEEE, May 2023, pp. 3308–3313. [Online]. Available: https://ieeexplore.ieee.org/document/10213898/

[12] Y. Han, G. Cheung, A. Li, C. R. Sullivan, and D. J. Perreault, "Evaluation of Magnetic Materials for Very High Frequency Power Applications," *Vabulas*, Jan. 2012, accepted: 2014-05-22T17:03:18Z Publisher: Institute of Electrical and Electronics Engineers (IEEE). [Online]. Available: https://dspace.mit.edu/handle/1721.1/87096

[13] J. G. Kassakian, D. J. Perreault, G. C. Verghese, and M. F. Schlecht, *Principles of Power Electronics*, 2nd ed. Cambridge, England: Cambridge University Press, Aug. 2023, ch. 25: Thermal Modeling and Heat Sinking.

[14] "Mag-Inc Ferrite Materials Datasheet," Aug. 2017. [Online]. Available: https://www.mag-inc.com/Media/Magnetics/File-Library/Products/Ferrite/Magnetics-Ferrite-Materials-Web-8-17a.pdf

[15] "TDK Ferrite Summary," Dec. 2021. [Online]. Available: https://product.tdk.com/system/files/dam/doc/product/ferrite/ferrite/ferrite-core/catalog/ferrite_summary_en.pdf

[16] G. Ahmed and M. Yovanovich, "Experimental Study of Forced Convection From Isothermal Circular and Square Cylinders and Toroids," *Journal of Heat Transfer-transactions of The Asme - J HEAT TRANSFER*, vol. 119, Feb. 1997.